IOWA STATE UNIVERSITY
Digital Repository

Retrospective Theses and Dissertations

Iowa State University Capstones, Theses and Dissertations

1995

Tissue characterization using A-mode ultrasound for beef quality grading, 1992-1995

Alpesh B. Patel
Iowa State University

Follow this and additional works at: https://lib.dr.iastate.edu/rtd

 Part of the Electrical and Electronics Commons

Recommended Citation
Patel, Alpesh B., "Tissue characterization using A-mode ultrasound for beef quality grading, 1992-1995" (1995). *Retrospective Theses and Dissertations*. 244.
https://lib.dr.iastate.edu/rtd/244

This Thesis is brought to you for free and open access by the Iowa State University Capstones, Theses and Dissertations at Iowa State University Digital Repository. It has been accepted for inclusion in Retrospective Theses and Dissertations by an authorized administrator of Iowa State University Digital Repository. For more information, please contact digirep@iastate.edu.

www.manaraa.com

Tissue characterization using A-mode ultrasound for beef quality grading

1992-1995

by

Alpesh Babubhai Patel

A Thesis Submitted to the

Graduate Faculty in Partial Fulfillment of the

Requirements for the Degree of

MASTER OF SCIENCE

Department: Electrical and Computer Engineering
Major: Electrical Engineering

Approved:
Signature redacted for privacy

Members of the Committee:
Signature redacted for privacy

Iowa State University
Ames, Iowa

1995

DEDICATION

To my grandfather, Kanubhai Patel, my friend and mentor, who is no longer with me in this world, whose intuition and ability to share his past at precise moments when he sensed I was searching for direction and meaning in life were very special.

To my parents, Babubhai Patel and Pravinaben Patel: you are two unique, independent, and creative individuals with a knack for taking the monotony out of life. I must try to find words to express the profound gratitude I owe you for your unwavering support and encouragement throughout my academic endeavors. You will always be with me.

TABLE OF CONTENTS

CHAPTER 1

INTRODUCTION

Many of the modern medical diagnostic and material characterization technologies are a direct result of clever use of ultrasound. Ultrasound, for example, is used very widely as a tool for characterizing tissue in medical applications. It is also used extensively in other applications such as nondestructive testing and fluid flow measurements. The objective of the research described in this thesis is to develop a computer based ultrasound system for characterizing beef tissue for quality grading.

Extensive research has been performed with regard to tissue characterization in medical applications. Similar work has also been carried out using ultrasound for structural analysis in material science applications. However, little has been done in applying ultrasound for characterizing beef tissue (quality grading). Thus, the requirements of an ultrasound system and the data processing algorithms are unknown. However, since beef tissue has physical properties that are similar to human tissue, the instrumentation and algorithms for analysis should be similar. This thesis describes the work and results obtained to date in attempting to achieve the stated objective.

The following section reviews the basics of ultrasound theory and application followed by a brief background on beef quality grading. Chapter two describes the PC-based system and the associated software developed for field data acquisition. Signal processing techniques used for extraction of frequency-domain and time-domain parameters are described in chapters' three and four, respectively. Chapter five briefly reviews basics of the statistical analysis and discusses the approaches used for parameter analysis and subsequent model development. Chapter six discusses the results obtained and presents directions for future research in the area.

Review of Ultrasound Theory and Applications

The theory and application of sound waves for characterizing the structure of materials has been of great importance to the fields of medicine and material science. This section reviews the principles involved in ultrasound tissue characterization. Since the primary interest is in applying tissue characterization techniques to beef quality grading, a review of literature covering this application is also presented.

Review of principles of Ultrasound

In layperson terms, sound wave can be described as propagation of mechanical vibrations from one region in a medium to another region through mechanical interaction of the molecules in the medium. Ultrasound is the term used for describing sound waves with frequencies above 20 KHz. The frequency range of ultrasound for medical application is usually between 1 MHz and 20 MHz. In broad terms, the material under test is typically insonified and ultrasound signal scattered by reflectors in the object are analyzed [1, 2].

Ultrasound is typically injected in to the material using a piezoelectric transducer. The piezoelectric effect is a phenomenon whereby certain crystalline materials become electrically polarized when subjected to mechanical stress, or conversely, are physically deformed when subjected to an electric field. Pierre and Jacques Curie are credited with the discovery of piezoelectricity. As a result of their discovery, early transducers were constructed from natural piezoelectric crystals such as quartz, tourmaline, and Rochelle salt. Modern ultrasound transducers are constructed with many different man-made ceramics and polymers such as lead zirconate titanate (PZT), poly vinylidine fluoride (PVDF). All of them are designed to convert the electrical signal to sound waves or vice-versa.

Piezoelectric crystalline are anisotropic. This means that piezoelectric effect can only occur in materials which lack a center of symmetry. The electric charges bound within the ionic

lattice of the material can interact with an applied electric field, to produce a mechanical effect. Conversely, if the crystal structure is subjected to stress, the electric charges can undergo large measurable changes. Thus piezoelectricity provides a coupling between electric and dielectric phenomena. To utilize these properties, electrical connections are made to the piezoelectric material by depositing metallic electrodes on opposite faces of the crystal. When the electrical connections are made to a time-varying voltage source, the mechanical deformations of the crystal produce sound waves that leave both metallized faces of the transducer. If a brief burst of electrical energy is applied to the electrodes, the crystal will vibrate resulting in propagation of sound waves into the medium with which the crystal is in contact. Similarly, a sudden mechanical impact will cause the crystal to produce a damped output signal. The most efficient transduction of energy occurs at the crystal's natural resonance frequency. This is determined in part by thickness of the crystal; the thinner the crystal , the higher the natural resonance frequency.

The acoustic waves (sound beam) that leave the radiating face will travel through a homogeneous medium in a coherent manner (i.e., it maintains the approximate lateral dimensions) until a distance is reached where natural divergence begins to spread the transverse extent of the beam. Figure 1 shows the side view of the ultrasonic beam for a disc transducer.

As seen in the figure, there is a critical distance where the field suddenly spreads out. This distance separates two distinct field types. The coherent field is called the Freznel zone or "near field" whereas the divergent region is called the Fraunhofer zone or "far field". The distance between the radiating face and the line dividing the two fields was shown to be

$$d = \frac{r^2}{\lambda}, \qquad \ldots(1)$$

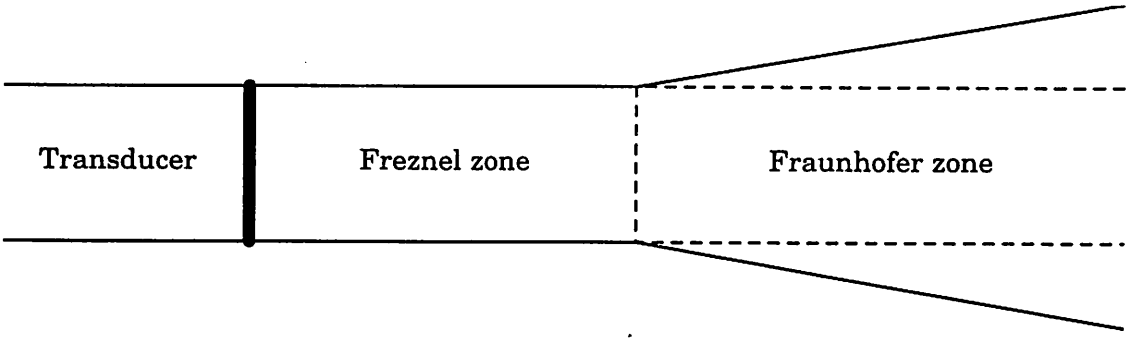

Figure 1. The Ultrasonic field of a plane disc transducer.

where d is the distance from the radiating face, r is the radius of the transducer face, and λ is the acoustic wavelength in the medium [1, 2].

Ultrasound Interactions

The acoustic wavelength is dependent on the velocity of sound in the medium and the frequency of the waves. Sound waves travel at approximately 331 m/s in air but their speed is much higher in denser media. A 1000 Hz tone has a wavelength of 0.31 meters in air and 1.5 meters in water.

Acoustic impedance is the resistance exerted by the material to sound propagation. It depends on the density and the velocity of sound in the material. Sound waves are reflected from the discontinuities in the structure. Some of the energy continues through the interface and some energy is returned back towards the source. The amount of energy returned depends on the angle of incidence of the wave at the interface and the difference in the acoustic properties of the media at the interface. The reflections from a large flat surface reflecting a perpendicularly incident beam are known as *specular reflections* whereas reflections from non-perpendicular sound beam incidence are known as *refractions*. The amount of energy reflected from a particular interface is measured in terms of the ratio of the reflected wave characteristic

impedance to the incident wave characteristic impedance. This ratio is also known as reflection coefficient (R) and can be expressed as

$$R = \frac{P_R}{P_I} = \frac{Z_1 - Z_2}{Z_1 + Z_2}, \qquad \ldots(2)$$

where Z_1, and Z_2 are the impedance of the materials making the interface, and P_1 and P_2 are pressure amplitudes of the incident and reflected beams, respectively.

The incident wave is reflected in all directions if the size of the interface is comparable to the magnitudes of the wavelengths. Such a phenomenon is known as *scattering* and the waves are said to be scattered. If the dimensions of the scattering objects are very much less than the wavelength then the resulting scattering is known as *Raleigh scattering*. Since the scattered wave spreads in all directions, echo signals detected from a volume containing small scatterers are not highly dependent on the orientation of individual scatterers. This is in contrast to the strong orientation dependence seen for specular reflection. The ratio of amount of energy scattered back to the source relative to incident energy, per unit area is defined as *backscatter coefficient*. Examples of scatterers are red blood cells and multiple air-filled alveoli of lung tissue.

The amplitude and intensity of a propagating ultrasound wave decrease as an exponential function of distance. This loss of energy by ultrasonic beam in the form of absorbtion and scattering is known as attenuation. The attenuation of energy is the result of interaction between ultrasound and the material. Attenuation is defined in terms of attenuation coefficient which can be expressed as

$$A = A_0 e^{-\alpha(f)\,l} \qquad \ldots(3)$$

Table I. Acoustic attenuation at 1 MHz for few common materials.

MATERIAL	ATTENUATION (dB/cm)
Water	00.0022
Aluminum	00.0180
Fat	00.6300†
Muscle	01.3000
Bone	20.0000

†Mean value at room temperature.

$$\alpha(f)=\beta_0 f^{\eta}, \qquad \ldots(4)$$

where l is the acoustic path length in the attenuating medium, A_0 is the amplitude at $l = 0$, η is the power of the frequency dependence of α, and β_0 is a constant.

As seen from these equations, the attenuation increases with increasing frequency thereby limiting the maximum frequency that can be used to scan the region at particular depth of the material or tissue. The working frequency range of ultrasound for tissue characterization is typically 1-5 MHz. Thus, attenuation indirectly limits the range of the resolution. Table I shows the attenuation of sound in various materials at a frequency of 1 MHz. Since, the attenuation is the parameter of interest in this study, it is discussed further in chapter three.

Ultrasound Applications for Tissue Characterization

The radio-frequency (RF) signal reflected and scattered from tissue can be displayed in the form of echo amplitudes as a function of time (or distance traveled in the tissue) which is known as A-mode representation or signals (Figure 2). Several such A-mode signals placed adjacent to each other provide information about the cross-section of the tissue. This can be displayed as a gray-scale image, known as B-mode ultrasound image.

Tissue characterization based on the analysis of reflected ultrasound (RF signal) includes estimation of propagation characteristics (velocity, attenuation, backscatter, etc.) by

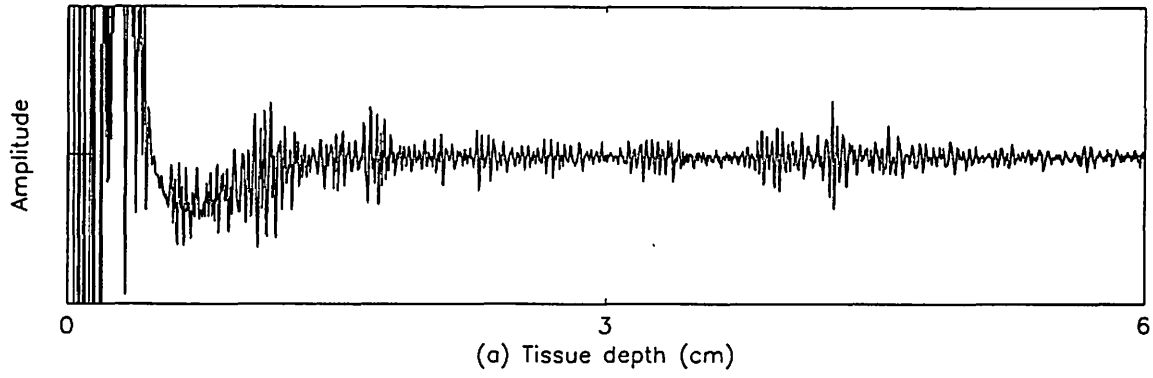

Figure 2. Typical A-mode signal obtained from muscle tissue.

various methods such as diffraction techniques, quantitative backscatter analysis, and spectrum analysis. It uses information present in the RF signal to detect, identify, or evaluate the tissue of interest. Qualitative or Quantitative interpretation of available information from A-mode signals and B-mode images has applications ranging from detection of fetus in the uterus to differentiation of pathologies of liver, breast, and eye [3]. A study of usefulness of acoustic properties in differentiating normal and cancerous human liver can be found in [4]. Reference [5] shows the potential for differentiation of histologically different types of melanomas by means of quantitative acoustic texture parameters.

Ultrasound has also been found useful in animal applications. It has been used for evaluating meat animals for many years but its use became widespread only in last decade. In its early stage, a single transducer was used to measure the thickness of the subcutaneous fat layer at one point (A-mode). By 1990, a real time scanner (B-mode) with a 17 centimeter long transducer was available commercially to image a complete cross section of longissimus dorsi (ribeye) muscle and was used to measure the cross-sectional area of the muscle.

For many years the beef industry has emphasized the need of developing an objective method for beef quality grading. Currently, the United States Department of Agriculture (USDA) follows a subjective method for beef carcass quality grading which primarily involves

visual inspection of content and distribution of intramuscular fat (or marbling). Marbling has been well established as an important quality attribute determining the ultimate palatability of meat. The marbling as seen on the cross-section of the ribeye (Longissimus dorsi) muscle between the 12th and 13th ribs is graded, from high to low marbling, as U.S. Prime, U.S. Choice, U.S. Good, and U.S. Standard by the USDA certified inspectors. This subjective method, however , does not meet the meat industries demand for value-based marketing system. To make the value-based marketing system a reality, there must be a process to objectively and non-invasively measure beef quality and composition in carcasses as well as live animals. One important step towards attaining this objective is characterizing intramuscular fat or marbling using ultrasound.

The ultrasound tissue characterization can be regarded as one of the pattern recognition problems in which several parameters are derived from ultrasound data (A-mode signals or B-mode images) and a consistent pattern or *tissue signature* is sought which characterizes a particular property of the tissue, e.g., intramuscular percentage fat (%-fat) in our study. It has been shown that features extracted from B-mode ultrasound images of the ribeye muscle can effectively predict intramuscular %-fat in live animals [6] as well as in carcasses [7]. These features were based on texture analysis of images. Since distribution of intramuscular fat gives a distinctive texture pattern in B-mode images, quantifying the texture could provide an objective method of evaluating %fat. Tissue characterization using A-mode ultrasound includes frequency-domain and time-domain analyses to estimate features of ultrasound/tissue interaction such as velocity, attenuation, and backscatter. A brief overview of different ultrasonic techniques used for tissue characterization can be found in [3].

Signal Processing Techniques

Several A-mode parameters have been shown effective for characterizing tissues. For example, kurtosis of gain-compensated backscattered signals has been reported to provide

discriminatory information for distinguishing fatty infiltrated liver from normal liver [8]. Spectral analysis of backscattered signal has been a very effective tool for deriving the parameters of tissue characterization [3, 9]. It provides a statistically meaningful technique for characterizing complex tissue structures. Attenuation of ultrasound has also been studied extensively for tissue characterization [10]. It has been applied for diagnosing diffuse liver diseases such as cirrhosis, hepatitis, and fatty infiltration. The envelope parameters have also been shown to be useful in tissue characterization. Some investigators have characterized various forms of heart diseases using statistical properties of envelopes of ultrasonic echoes from the myocardium [11].

CHAPTER 2

DATA ACQUISITION AND ANALYSIS SYSTEM

A personal computer (PC) based system was developed for ultrasonic data acquisition using the pulse-echo (A-mode) configuration. It was designed for on-line field data acquisition. Figure 3 illustrates the modules employed in the system. A commercially available 12.5 cm long linear array transducer was used to transmit as well as receive the ultrasound signals. The transducer had 72 elements, each operating at a frequency of 3.5 MHz. The ultrasound a center frequency of 3.5 MHz provided with enough tissue penetration and adequate axial resolution.

An ultrasonic pulser/receiver (IPR-90, Physical Acoustic Corporation, Princeton, New Jersey) plug-in board along with two 8-channel multiplexer boards (MUX4800, Sonix Incorporated, Springfield, Virginia) were used to sequentially trigger sixteen channels (in groups of four elements) of the transducer. The pulser provided an impulse for driving the piezoelectric transducers at a fixed rate, called pulse repetition rate. Pulse repetition rate was kept at 1 KHz at a fixed pulse width of 0.5 nsec. The pulser voltage which drives the transducer was kept constant at 200 volts. The receiver detects and amplifies the echoes. The receiver gain and attenuation settings were kept constant at 40 dB and 20 dB, respectively. The fraction of time the transducer is actually emitting or receiving is indicated by *duty factor*, which is a dimensionless quantity representing the ratio of the pulse repetition rate (pulses/sec) and the time duration of each pulse (sec/pulse). The multiplexer boards provide controls for switching from one channel to another.

A digital oscilloscope (LeCroy 9310L, LeCroy, Chesnut Ridge, New York) was used for acquiring the data from the pulser/receiver and then transferring the data to the PC using the GPIB interface (IEEE 488 standards). An interactive software was developed using C language to control the pulser/receiver, multiplexer, and the GPIB boards. The task for data acquisition

included opening/closing of selected multiplexer channels, triggering selected transducers and transferring the digitized signals from the oscilloscope to the computer hard disk using the GPIB board. The signals were sampled at a rate of 20 MHz using a 256-level (8-bit) quantizer resident in the oscilloscope. This sampling rate provided good resolution and also satisfied the Nyquist criteria.

A total of 311 wet carcasses were scanned immediately after slaughter and hide removal at a commercial packing facility. After cutting a slit through the fat layer across the 11^{th}-13^{th} ribs, the transducer was placed in good contact with the ribeye muscle. This oriented the ultrasound beam in a direction that was perpendicular to the muscle fibers. Sixteen A-mode signals, each of record length equivalent to about 8 cm of tissue (based on ultrasound velocity of 1540 m/s for soft tissues and 20 MHz sampling rate), were acquired for each carcass. Typical signals from low and high %-fat muscles are shown in Figure 4. The ribeye slices between 12^{th} and 13^{th} ribs were later processed chemically at Iowa State University Meat Laboratory to determine the actual intramuscular %-fat using the n-hexane extraction method. This actual %-fat was later used to correlate with the parameters extracted by applying signal processing algorithms. All the A-mode signals acquired were transferred to a computer workstation (DECstation 5000, Digital Equipment Corporation, Maynard, MA) for processing.

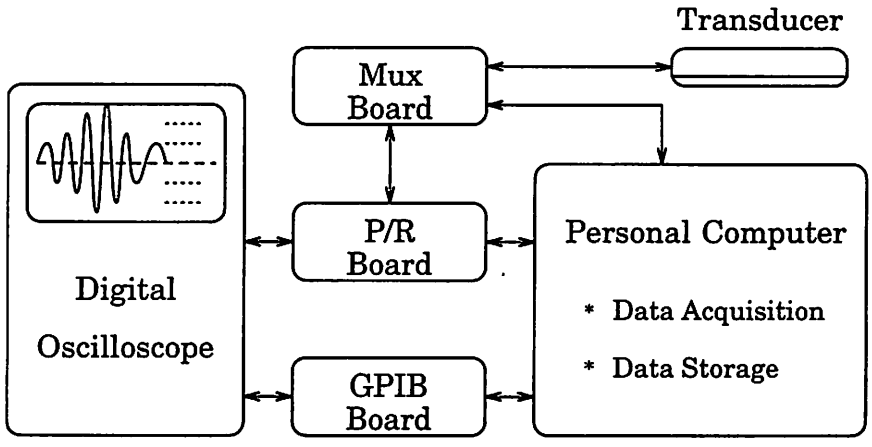

Figure 3. Block diagram of the data acquisition system.

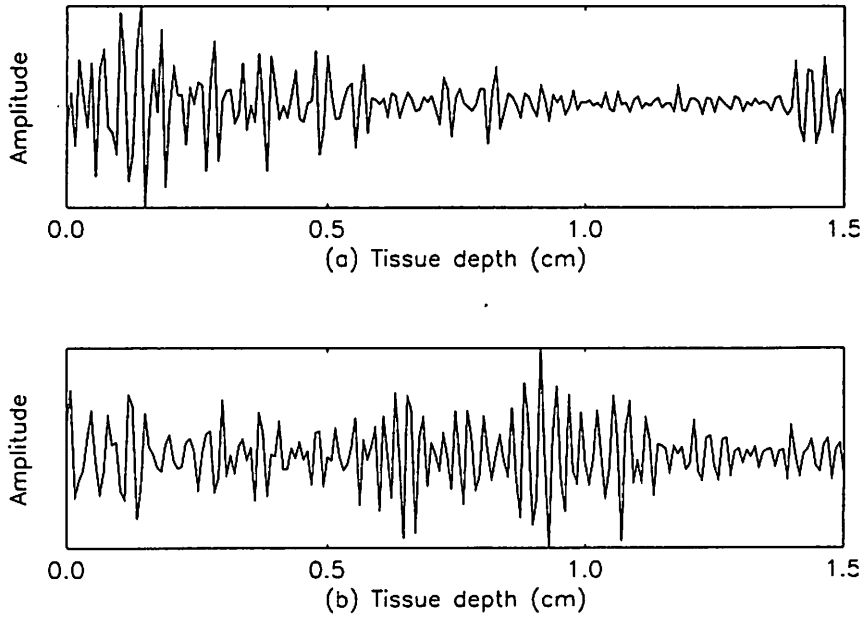

Figure 4. Typical A-mode signals (arbitrary amplitude units) from ribeye muscle (a) low (4.25) %-fat (b) high (7.56) %-fat.

CHAPTER 3

FREQUENCY-DOMAIN PROCESSING

Spectral Parameters

The first step in spectral feature (parameter) extraction is the estimation of the spectrum. Many spectral estimation techniques such as periodogram [12, 13], linear models [14], maximum likelihood approaches [15], and subspace methods [15]. have been proposed.

The periodogram, P(k), of a stationary random signal, x(n), can be computed as

$$P(k) = \frac{1}{LU}\left|N\text{–point DFT}\{w(n)x(n)\}\right|^2, \qquad \ldots(5)$$

where w(n) is the rectangular window of length L and U is the normalization factor for removing the bias in the spectral estimate. The DFT indicates discrete fourier transform which is commonly implemented using an efficient radix-2 fast fourier transform (FFT) algorithm. The periodogram is an inconsistent estimate as its variance does not approach zero with increasing the window lengths. In order to obtain a consistent estimate periodogram the spectra can be averaged. However, this would require that the signal be stationary and hence cannot be used in our application.

Spectral estimation based on linear models is a three step procedure. The first step is to select the model. The second step is to estimate the model parameters using the available data and the third step is to obtain the spectral estimate using the parameters estimated in the second step. One major motivation for the use of this approach is the apparent higher resolution that can be obtained. The degree of improvement in the resolution and spectral fidelity is determined by the accuracy of the assumed model with a small number of parameters. Any inaccuracy in the model will result in a bias in the spectral estimate. For the problem on hand,

no prior information about the underlying process is available and consequently, it would be unwise to use this method for spectral estimation. The maximum likelihood approaches for spectral estimation are computationally intensive and since high resolution is not necessary, they were not used.

Signal Analysis Using Fourier Transform

After reviewing the alternative methods and considering the fact that the characteristics of the A-mode signals (x(n)) change with time, a simple windowed Fourier transform method was used. The signal x(n) is typically multiplied by a finite-duration window, w(n), since the input to the discrete Fourier transform must be of finite duration. The effect in the frequency domain is a periodic convolution, i.e.,

$$V(e^{j\omega}) = \frac{1}{2\pi}\int_{-\pi}^{\pi} X(e^{j\theta})W(e^{j(\omega-\theta)})d\theta, \qquad \ldots(6)$$

where, $X(e^{j\omega})$ and $W(e^{j\omega})$ are the Fourier transforms of x(n) and w(n), respectively. If w(n) is constant over the range of n for which it is nonzero, it is referred to as a rectangular window. However, it is better to taper the window at its edges as it reduces the amplitude of the sidelobes. In addition to this effect, tapering at the edges results in a wider mainlobe leading to a wider transition band at the discontinuities of the desired frequency response.

The primary purpose of windowing the signal is to limit the extent of the signal to be transformed so that the spectral characteristics are reasonably stationary over the duration of the window. It should also be noted that the more rapidly the signal characteristics change, the shorter the window should be. However, this reduces the frequency resolution. On the other hand, as the window length decreases, the ability to resolve changes with time increases. Consequently, the choice of window length becomes a trade off between frequency- and time-resolution. In addition, windowing a signal smears or broadens the impulses in the theoretical

Fourier representation and thus the exact frequency is less sharply defined. It also reduces the ability to resolve the signals that are closely spaced in frequency. The spectral sampling inherent in the DFT also has the effect of potentially giving a misleading or inaccurate picture of the true spectrum of the signal. The width of the mainlobe of the discrete Fourier transform of the window, W(k), primarily influences the resolution whereas the relative amplitude of the mainlobe and the sidelobes of W(k) affect the degree of spectral smearing. In our case, the signals were windowed using two windows of two different lengths and were analyzed in a similar manner.

The following paragraph discusses the extraction of the spectral parameters from the backscattered radio frequency (RF) signals based on the convolution model. The RF signal arising due to reflections from the tissue scatterers can be modeled as

$$x(n) = e(n) * i(n) * g^2(n) * a^2(d,n) * \mu(d,n), \qquad \ldots(7)$$

where, e(n) is the electrical impulse applied to the piezoelectric transducer, i(n) is the electroacoustic response of this transducer, g(n) is the diffraction impulse response, a(n) characterizes the acoustic attenuation, and $\mu(n)$ is the scattering function. It should be noted here that the transducer is assumed to be sufficiently small such that the diffraction effects may be assumed to be constant in space. The temporal window is also assumed to be sufficiently short, lying at a mean distance d from the transducer, such that the attenuation may be assumed to be nearly position independent. Equation (7) can be rewritten as

$$x(n) = e(n) * j(n) * \mu(d,n), \qquad \ldots(8)$$

where j(n) is defined by

$$j(n) = i(n) * g^2(n) * a^2(d,n). \qquad \ldots(9)$$

By taking the discrete Fourier transform of equation (8), we have

$$X(k) = E(k)J(k)M(d,k). \qquad \ldots(10)$$

This expression summarizes the fact that the spectrum of the RF signal is constituted by a constant spectrum associated with the transducer, multiplied by a filtering function carrying information about diffraction and attenuation in the tissues, and again multiplied by a function representing information about the tissue scatterers. The last two functions are important for characterizing the tissue. But since the information relating to the scatterers (M(d, k)) is not available, only the J(k) function can be isolated and interpreted for characterization. In this study, the contribution M(d, k) was suppressed using homomorphic filtering techniques. The spectral parameters were extracted based on E(k) and J(k). Since, E(k) was kept same for all the signals, the spectral parameters essentially represent J(k). The next paragraph discusses the techniques used for extracting the spectral parameters from the data.

Each backscattered signal, x(n), was windowed at a depth of about 3.45 cm using a Hanning window of 12.78 μs duration so as to analyze the central region of the ribeye muscle. The length of the window was equivalent to a window size of 256 points or about 0.99 cm of the tissue. The spectrum of each of 16 windowed signal-segments from a muscle was computed by using the Fast Fourier Transform (FFT) algorithm given by

$$X(k)=\sum_{n=0}^{N-1} x(n)w(n)e^{-j2\pi kn/N}, \qquad 0 \le n \le N-1 \qquad \ldots(11)$$

where x(n) is the filtered signal and w(n) is the Hanning window, of size N, defined as

$$\begin{aligned} w(n) &= 0.5 - 0.5\cos(2\pi n/N), && 0 \le n \le N-1 \\ &= 0, && \text{otherwise.} \qquad \ldots(12) \end{aligned}$$

The log-squared magnitude of X(k) was then computed and 16 such spectra were averaged (point-to-point) to obtain a single raw power spectrum, $S_R(k)$, for each carcass, as shown in Figure 5 (b) and (c). The raw power spectrum is defined as

$$S_R(k)=\frac{1}{16}\sum_{i=1}^{16}\left\{10\log_{10}\left[|X(k)|^2\right]\right\}, \qquad 0\le k\le N-1. \qquad \ldots(13)$$

Examining Figure 5 (b) and (c), we note that $S_R(k)$ consists of a rapidly varying component added to a more slowly varying component. The rapidly varying component is due to reflections from the scatterers and provides information about the scatterer density and distribution. The slowly varying component is due to the transducer response, diffraction impulse response, and attenuation and primarily provides information about the frequency shift due to acoustic attenuation. As stated earlier, information about the scatterers is not required and hence, $S_R(k)$ was smoothed by filtering in the cepstral domain using homomorphic filtering techniques [12]. The cepstrum of the raw power spectrum, $S_R(k)$, was computed by taking its inverse Fourier Transform. The cepstrum was then subjected to a lowpass frequency-invariant linear filter of length equal to 11 points. A filter F{.} that transforms an input sequence P(f) into an output sequence Q(f) is called a linear frequency-invariant filter if it has the following properties:

1. Scale Preservation: $F\{\alpha P(f)\}=\alpha F\{P(f)\}.$

2. Superposition: $F\{P(f_1)+P(f_2)\}=F\{P(f_1)\}+F\{P(f_2)\}.$

3. Frequency Invariance: if $F\{P(f)\}=Q(f)$, then $F\{P(f+\zeta)\}.=Q\{f+\zeta\},$

where, ζ is integer-valued. Filters of longer length tend to over-smooth the spectra whereas smaller length filters tend to under-smooth the spectra. A the filter of length 11 points was

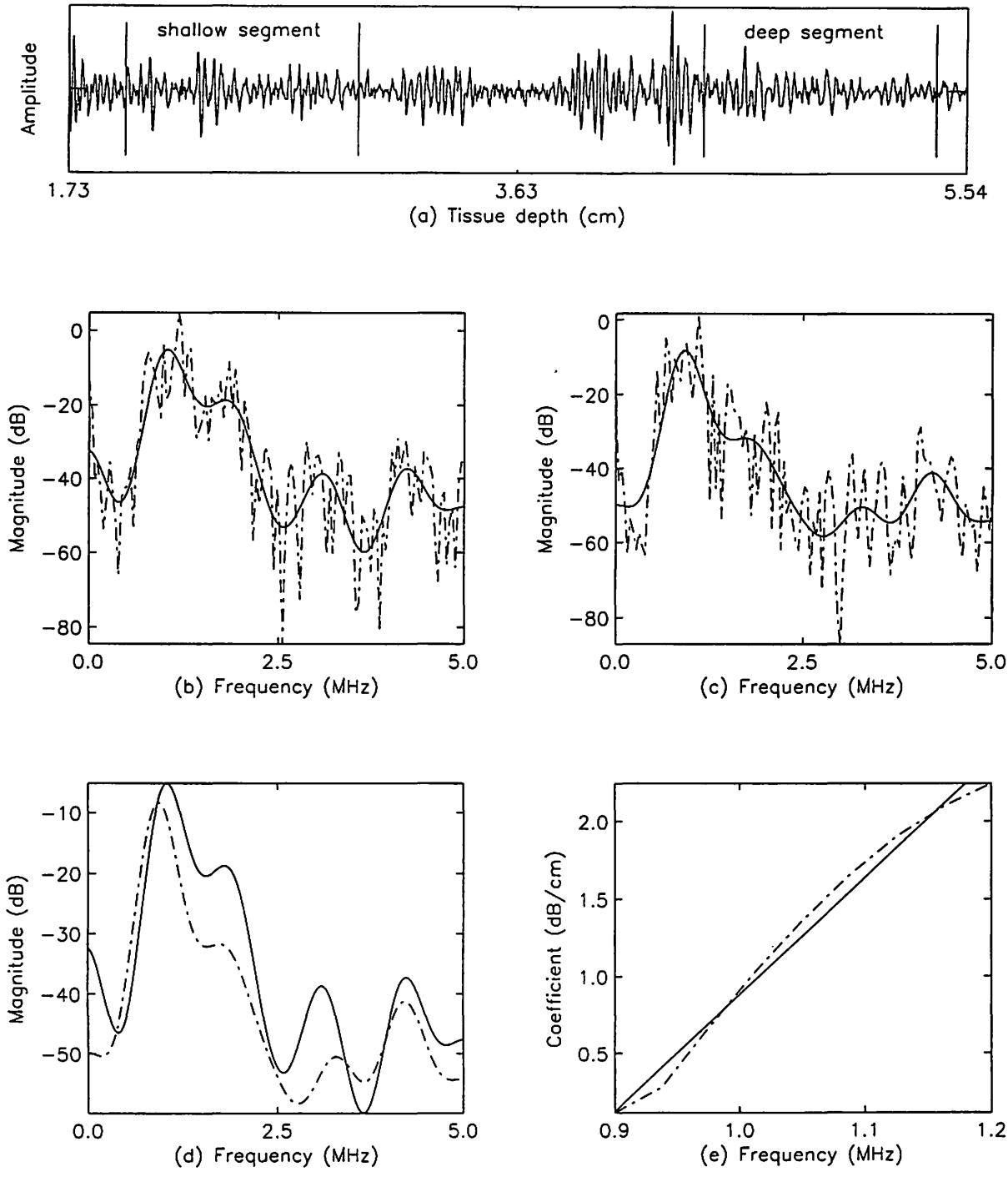

Figure 5. (a) Typical signal with shallow and deep segments. (b) & (c) Raw (dotted line) and smooth (solid line) power spectra of the shallow and deep segments, respectively. (d) Comparison of shallow and deep power spectra. (e) Attenuation coefficient log-spectral difference within bandwidth as a function of frequency.

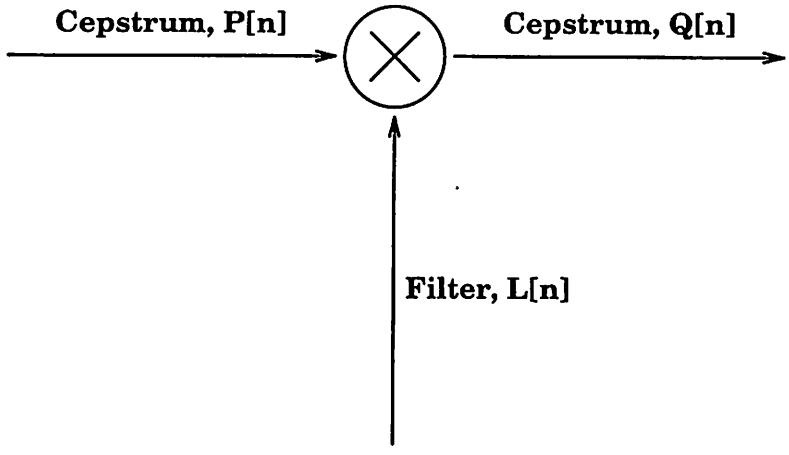

Figure 6. Time domain representation of frequency invariant filtering.

found to provide adequate smoothing in this case. The frequency-invariant linear filter can be implemented by convolving the functions in the frequency domain or, as illustrated in Figure 6, by multiplication in the time domain. Figure 7 shows the time response of frequency-invariant, lowpass, linear system required for estimating the product of E(k) and J(k). The output is then transformed to the Fourier spectral domain as shown in Figure 5 (b) and (c).

The six-dB bandwidth of the smoothed spectrum, $S_s(k)$, was computed to obtain the 6-dB low cutoff frequency (f_L) and 6-dB high cutoff frequency (f_H). A third parameter, center frequency (f_C), was computed using the centroid formula

$$f_C = \frac{\sum_{k=f_L}^{f_H} k|S_s(k)|^2}{\sum_{k=f_L}^{f_H} |S_s(k)|^2}. \qquad \ldots(14)$$

Additional parameters calculated from $S_s(k)$ within the bandwidth were: total power (P_T), average power (P_A), peak power (P_P), and frequency at peak power (f_P). Thus, 7 spectral parameters were calculated for each carcass ribeye muscle. In order, to study the effect of

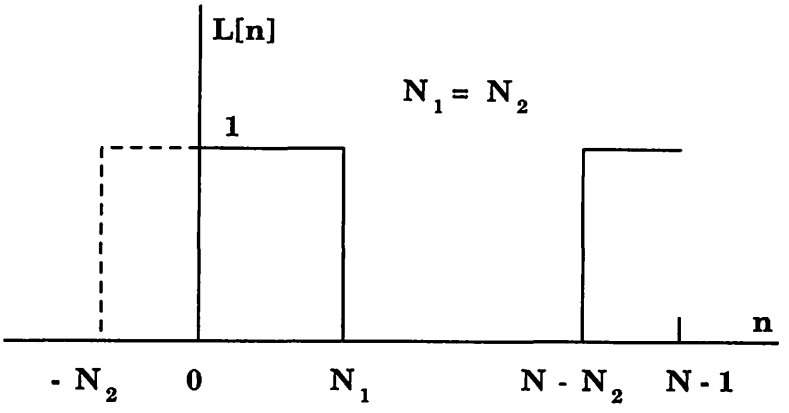

Figure 7. Time response of the lowpass filter.

window length, a larger (512-point) window centered at the same depth (3.45 cm) was used to extract the signal segment and all the spectral parameters were recalculated.

Attenuation Parameters

Attenuation can be defined as loss of energy suffered by the ultrasonic beam. The losses include those caused by absorption and scattering. Many methods have been proposed and used for measuring ultrasonic attenuation [3]. The log spectral difference method is used in our study since it eliminates the responses of the transducer, the electronic system, and the tissue overlaying the region of interest. The power spectra from two depths, L_1 (shallow) and L_2 (deep), can be related through

$$|X_2(\omega)|^2 = |H(\omega)|^2 |X_1(\omega)|^2, \qquad \ldots(15)$$

where $|X_1(\omega)|^2$ and $|X_2(\omega)|^2$ are the power spectra of the shallow and deep signal-segments, ω represents continuous frequency axis, $|H(\omega)|^2$ is the power transfer function which, in general includes all the processes contributing to transform the power spectrum measured at depth L_1 to that measured at depth L_2 [16]. In equation (15) we assume that the ensemble of scattering

particles distributed at depth L_1 have the same scattering properties as the particle distribution at depth L_2. If attenuation were the only transformation process, then

$$|H(\omega)|^2 = e^{-2\alpha(\omega)\Delta L}, \qquad \ldots(16)$$

where $\alpha(\omega)$ is frequency-dependent amplitude attenuation coefficient [17] and ΔL is path length between depth L_1 and depth L_2. Solving equations (15) and (16) for the attenuation coefficient, $\alpha(\omega)$, yields

$$\alpha(\omega) = \log\left[\frac{|X_1(\omega)|^2}{|X_2(\omega)|^2}\right] \Big/ (2\Delta L). \qquad \ldots(17)$$

It should be noted here that the beam diffraction effect is ignored since the same transducer and system were used and our primary purpose was to determine the relative attenuation differences across the muscle samples. Figure 5 illustrates the steps involved in this method. A shallow and a deep segment were Hanning windowed from the backscattered A-mode signal (Figure 5 (a)). The smooth power spectra were obtained in a similar way as described earlier(Figure 5 (b) and (c)). Here, averaging of spectra over a depth plane of tissue has been shown to improve the estimates of the attenuation parameters [18]. Averaging of spectra is necessary since the attenuation is affected by inhomogeneous nature of the tissues and random changes in the size, shape, and correlation length of the scatterers. The windows (time gates) were 256-point (12.78 μs) long and were centered at tissue depths of 2.46 cm and 4.92 cm. The attenuation coefficient, $\alpha(k)$, was then computed using equation (17) (Figure 5 (d) and (e)).

Two models for frequency dependence of $\alpha(k)$ were used to calculate the four attenuation parameters:

Linear fit model: $\alpha(k) = A_1 + A_s\, k$

power-law model: $\alpha(k) = B_0\ k^{\eta}$

where k represent the discrete frequency points, A_I is the intercept and A_S is the slope as determined by fitting a straight line to the $\alpha(k)$ curve (Figure 5 (e)), and B_0 is the coefficient and η is the power of frequency dependence as determined by fitting a power-law model to the $\alpha(k)$ curve. Only these two models were fitted as there is no good theoretical basis for describing the functional relationship between attenuation and frequency in tissues. A number of relationships have been proposed but most of the reports have indicated that the power law model of the form indicated describes the frequency dependence very well.

Thus, 18 parameters were calculated using frequency-domain processing for the purpose of tissue characterization:

- 7 spectral parameter for 256-point window,
- 7 spectral parameter for 512-point window, and
- 4 attenuation related parameters.

CHAPTER 4

TIME-DOMAIN PROCESSING

Kurtosis Parameters

The kurtosis, K, is defined as the normalized fourth central moment of a random variable which in our case is the filtered A-mode signal. The kurtosis is given by

$$K = \frac{E[x^4]}{\{E[x^2]\}^2}, \qquad \ldots(18)$$

where x is a zero-mean random variable and E[.] is an expectation operator. For a uniformly distributed process K is equal to 1.8, while for Gaussian and Laplacian processes it is equal to 3 and 6, respectively (Figure 8). This implies that K provides a measure of the "peakiness" of a signal, e.g., backscattered RF signal. The estimator $K_E(n)$ for an observed data sequence denoted by x(n) can be defined as

$$K_E(n) = \frac{\frac{1}{M}\sum_{n=1}^{M} x(n)^4}{\left\{\frac{1}{M}\sum_{n=1}^{M} x(n)^2\right\}^2} = \frac{M\sum_{n=1}^{M} x(n)^4}{\left\{\sum_{n=1}^{M} x(n)^2\right\}^2}, \qquad \ldots(19)$$

where we replace the ensemble average in equation (18) by the time average. It has been shown that, for the estimator $K_E(n)$ to be an unbiased estimator, it is necessary that the random process be stationary to at least the fourth moment. Hence, for ultrasonic backscattered signal, which is a non-stationary sequence, an automatic gain control (AGC) has been suggested to compensate for variations in the amplitude [8].

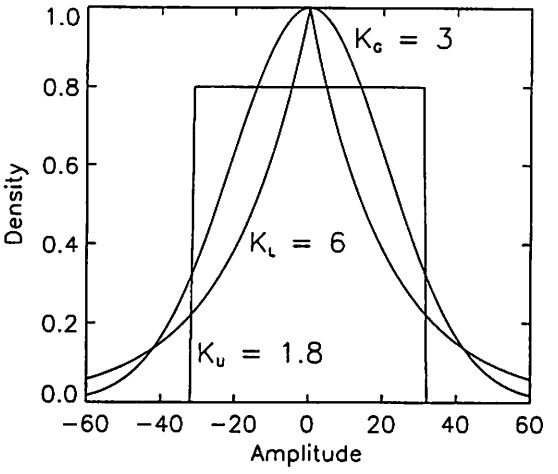

Figure 8. Gaussian, Laplacian, and Uniform probability density functions and their kurtosis values, K_G, K_L, and K_U, respectively.

The AGC algorithm is implemented by calculating the average energy of the signal, denoted by E(n), in an interval around a point n and then applying a gain to the signal that tends to maintain a constant energy level. E(n) is determined from a weighted sum of the absolute values of the preceding and succeeding N/2 samples:

$$E(n)=\frac{1}{N+1}\sum_{k=0}^{N}\left|x(n+k-N/2)w(k)\right|, \qquad \ldots(20)$$

where w(k) is the Hamming data window defined as

$$w(k)=0.54-0.46\cos\left(\frac{2\pi k}{N}\right), \qquad 0\le k\le N$$
$$=0, \qquad \text{otherwise.} \qquad \ldots(21)$$

The data window was applied to de-emphasize the contribution due to the introduction and deletion of the sample values at the extremes of the data interval. The AGC gain at point n is set equal to 1/E(n), and the output signal is then given by

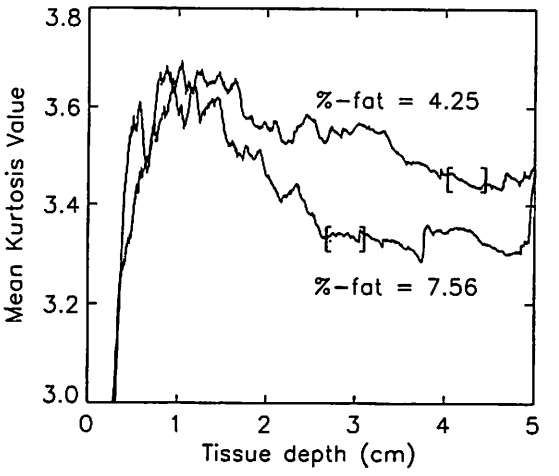

Figure 9. Typical plots of kurtosis estimator $K_E(n)$ for the signals from low and high %-fat ribeye muscles.

$$y(n) = x(n)/E(n). \qquad \ldots(22)$$

The duration of the data window (N+1) is important because if N is chosen to be too small, then E(n) tends to vary rapidly with n and thus reduces the K value. On the other hand, if N is chosen too large, the amplitude variation in the signal is not compensated, and the signal remains non-stationary. A window size of 128 points represented a reasonable compromise for acquired ultrasound data. This window size represented tissue range increment of about 5 mm, based on an assumed ultrasonic velocity of 1540 m/s in soft tissue and a sampling rate of 20 MHz.

Each A-mode signal was preprocessed using a recursive Butterworth high pass filter to remove noise (below 0.2 MHz). The filtered signal was then subjected to a digital AGC algorithm using a 128-point Hamming window (representing about 0.5 cm of tissue) to assure a constant signal energy with tissue depth. The kurtosis estimator was then estimated using equation (19). By averaging (point-to-point) the kurtosis estimates from 16 A-mode signals, a single estimate $K_E(n)$ as a function of tissue depth was obtained for every carcass. Figure 9 presents typical

plots for two different %-fat muscles. From such curves, two parameters were calculated: a final stabilized kurtosis value (K_S) and the depth at which $K_E(n)$ stabilized (in terms of sample number, n_K.) The $K_E(n)$ value was considered to be stabilized or settled if consecutive $K_E(n)$ values showed fluctuations that were no more than 0.0001 for a 9-point sliding window.

Envelope Parameters

The filtered backscatter signals were Hanning windowed, in a similar way as described in the spectral parameters section, to obtain 256-point and 512-point signal segments. These signal segments were subjected to an envelope detection algorithm. This algorithm was implemented by shifting the phase of every component of the signal by $\pm\pi/2$ (using discrete Hilbert transform [12]) and then computing the envelope, E(n), as given by equation (23).

$$E(n) = \sqrt{\left(x[n]^2 + H\{x[n]\}^2\right)}, \qquad 0 \le n \le N-1. \qquad \ldots(23)$$

where H{x[n]} is the Hilbert transform of the filtered signal x[n]. Three parameters were extracted from the signal envelope: root-mean-square (rms) energy, the number of peaks, and mean of the histogram (H_M).

The averaged rms energy (E_G) was computed using equation (24) where rms energy is averaged over all the 16 signals.

$$E_G = \frac{1}{16}\sum_{i=1}^{16}\left\{\sqrt{\frac{1}{N}\sum_{n=0}^{N-1}\left|E[n]\right|^2}\right\}, \qquad 0 \le n \le N-1. \qquad \ldots(24)$$

This parameter may provide insight into the relationship between the intramuscular fat and the total scattering power which in turn depends on the number of scatterers and their scattering strength.

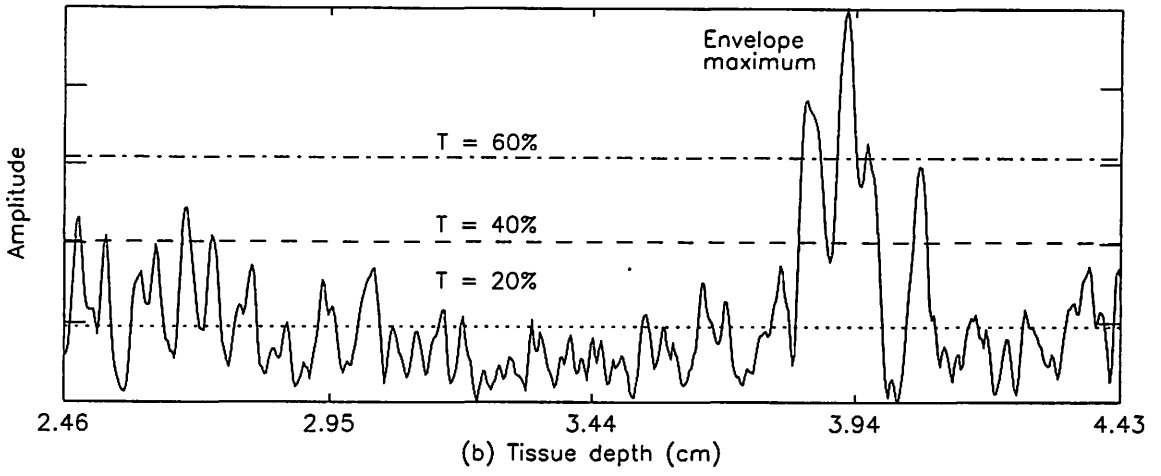

Figure 10. Envelope of a signal segment with 20%, 40%, and 60% thresholds.

The number of peaks were computed using a simple peak detection algorithm with varying threshold. The algorithm searches for a maximum having four sample points on either side with amplitudes greater than the threshold. This maximum was than recorded as a peak. In this way, the number of total peaks (P_1, P_2, P_3) with three different threshold values (20%, 40%, and 60% of the maximum value of the envelope, respectively) were computed and averaged over 16 signals. Figure 10 illustrates the procedure. The dependence of the thresholds on the maximum of the envelope of the signal segment should be noted. Our main interest here was in the backscatter from the scatterers within the region of interest, independent of the attenuation before the region of interest. Though empirical, these parameters are expected to provide some information about the density of the scatterers.

The mean of the histogram of the envelope amplitude was computed to observe its shift with variations in intramuscular fat. It was computed using equation (25) which gives the mean of the histogram averaged over 16 A-scans.

$$H_M = \frac{1}{16}\sum_{i=1}^{16}\left\{\frac{1}{N}\sum_{n=0}^{N-1}E(n)\right\}, \qquad 0 \le n \le N-1 \qquad \ldots(25)$$

Thus, two kurtosis based parameters and three envelope based parameters were calculated using time-domain processing for the purpose of tissue characterization. These parameters were used with the frequency-domain parameters for the development of a prediction model.

CHAPTER 5

STATISTICAL ANALYSIS

The signal parameters were further analyzed using statistical methods to develop models for predicting the intramuscular %-fat. All the analyses were done using the SAS package (SAS Institute, Inc., Cary, NC). The principles underlying the statistical analyses are briefly reviewed first. The specific details of statistical analysis performed on the data acquired is then discussed. Additional details on statistical analysis can be obtained from [19, 20, 21].

Pearson's Product Moment Correlation Coefficient

Consider a dependent variable, y, and an independent variable, x. When the variables x and y are linearly related, the correlation coefficient (r) is a measure of the degree of relationship present. It may be defined as the covariance of x and y, C_{xy}, divided by the product of the standard deviations of the x (S_x) and y (S_y) variables, or

$$r = \frac{C_{xy}}{S_x S_y}. \qquad \ldots(26)$$

Spearman's Rank Correlation Coefficient

Spearman's rank correlation coefficient (r_s) is the correlation coefficient between the ranked values of the variables. This is useful in examining the correlation in the data which is not normally distributed. The coefficient r_s can be computed by first finding the ranks of the variables separately and then computing the ordinary correlation coefficient between the ranked values of the variables. It can be efficiently computed using

$$r_S = 1 - 6\sum d^2 / \left[N\left(N^2 - 1\right)\right], \qquad \ldots(27)$$

where d is the difference between the ranks and N is the sample size.

Linear Regression

Linear regression is a means to estimate the relationship between a dependent variable, y, and an independent variable, x. The variability that the y exhibits has two components: a systematic part and a random part. The systematic variations of y can be modeled as a function of the x variable. The model relating y to x is called regression equation and can be written as $y = \beta_0 + \beta_1 x + \varepsilon$. The random part, ε, takes in to account the fact that model does not exactly describe the behavior of the response.

In case of Multiple linear regression, the response variable varies with a set of independent variables $x_1, x_2, \ldots x_m$. The general regression model can be expressed as

$$y=\beta_0+\beta_1 x_1+\beta_2 x_2+\ldots+\beta_m x_m+\varepsilon, \qquad \ldots(28)$$

where, y is the response or the dependent variable, $\beta_0, \beta_1, \ldots, \beta_m$ are unknown parameters, and ε is the random error term.

The Least squares technique is used to estimate the parameters. The goal is to find estimates of the parameters $\beta_0, \beta_1, \ldots, \beta_m$ that minimizes the sum of the squared differences between the actual y values and values of y predicted by the equation (28). These estimates are called least-squares estimates and the quantity minimized is called the error sum of squares.

A basic identity stemming from the least squares, specifically,

$$\sum(y-y_M)^2=\sum(y_M-y')^2+\sum(y-y')^2. \qquad \ldots(29)$$

This identity shows that the sum of squared deviations from the mean has two terms: the sum of the squared differences between the mean (y_M) and the predicted (y') values, and the sum of the squared differences between the observed (y) and the predicted (y') values. These two parts

are called the regression model sum of the squares (SS) and the residual (or error) sum of squares. Thus,

Corrected Total SS = Model SS + Residual SS.

Typically regression analysis is used for the following purposes:

- obtain the least-squares estimates of the parameters
- estimate the variance of the error term
- estimate the standard error of the parameter estimates
- test hypotheses about the parameters
- calculate the predicted values using the regression equation
- evaluate the fit or lack of fit of the model

Coefficient of Determination (R^2)

The coefficient of determination (R^2) is the square of the multiple correlation coefficient. For a one independent variable regression it is equivalent to the square of the correlation between the dependent variable and independent variable. The value of the R^2 is commonly interpreted as the portion of variance that x and y have in common. In other words, R^2 is the proportion of the y variance that can be accounted for by the linear regression of y on x and also the proportion of the x variance that can be accounted for by the linear regression of x on y. Since the predicted values are a linear function of the independent variable, it is also the square of the correlation between the dependent variable and its predicted values. Finally, it is also the ratio of Model SS divided by Total SS which can be expressed as

$$R^2 = \frac{\sum (y_M - y')^2}{\sum (y - y_M)^2}. \qquad \ldots(30)$$

Mallows Statistic

The Mallows statistic is used for selecting a subset of variables that carries the most amount of discriminatory information. A number of other statistics have been developed for this

purpose but this the most frequently used statistic. It is a measure of total squared error for a subset model containing p independent variables. The total squared error is a measure of the error variance plus the bias introduced by not including the important variables in the model. It may, therefore, indicate when too many variables are being excluded from the model. This statistic is computed as

$$C(p)=(SSE(p)/MSE)-(N-2p)+1, \qquad \ldots(31)$$

where MSE is the error mean square for the full model (or some other estimate of the pure error), SSE(p) is the error sum of the squares for the subset model containing p independent variables and, N is the total sample size.

For any given number of selected variables, larger C(p) values indicate equations with larger mean squares error. For any subset model C(p) > (p+1), there is evidence of bias due to an incompletely specified model. On the other hand, if there are values of C(p) < (p+1), the full model is said to be over specified, i.e., it contains too many variables. Mallows recommends selecting that subset size where the minimum C(p) first approaches (p+1), starting from the full model.

Root Mean Square Error (RMSE)

Root mean square error (RMSE) is the square-root of the mean square error. It can be expressed as

$$RMSE=\sqrt{\sum(y-y')^2/(n-m-1)}, \qquad \ldots(32)$$

where n is the number of observed values of y and m is the number of variables required for a complete model.

Test of Significance

In testing a null hypothesis for significance, the significance level, α, of the test is decided in advance. It is used as a basis for deciding whether or not to reject the null hypothesis. Frequently used thresholds are $\alpha = 0.05$ and $\alpha = 0.01$, but other values of α may also be chosen. If the result of the test of significance (i.e. the p value) is such that the probability of the outcome is equal to or less than α, then the null hypothesis is rejected. This simply means that the probability of the outcome is sufficiently small that we choose to regard the null hypothesis as improbable or false.

The tests of significance are commonly made by transforming a statistic or statistics based on a sample into another statistic for which the probability distribution is known, given that a null hypothesis is true. The commonly used distributions are the standard normal distribution, the t distribution, and the chi-square distribution.

Analysis of Ultrasound Parameters

The correlations of the ultrasound parameters with the actual %-fat were calculated in the form of the Pearson's product moment correlation coefficients (r_p) and Spearman's rank correlation coefficients (r_s). The parameters showing significant correlation with %-fat were selected for further analysis. The selection of parameters with high mutual correlation was avoided since they provide essentially similar information about the tissue properties. Next, a systematic analysis of the selected parameters was done seeking a multiple regression model which gave the maximum coefficient of determination (R^2), smaller Mallow's statistics, and the minimum residual error (for adequacy of the model) with significance level (p value) less than 0.05. For developing models of %-fat prediction, the data set (consisting of data from 311 carcasses) was divided into two groups. The first group with about 70% of the carcasses was used in the development of the prediction model and the second group with remaining 30% of

the carcasses was used for validating the prediction model. For validation, the correlation, regression, as well as residual analyses of predicted versus actual %-fat were done for each model.

CHAPTER 6

RESULTS AND DISCUSSION

Actual Intramuscular %-Fat

Of the 311 carcasses that were scanned, the actual %-fat data were available for 295 ribeye samples. The %-fat, as determined by the n-hexane method, ranged from 1.54% to 11.99%, with a mean value of 4.87% and standard deviation of 1.70%. This range included the %-fat found in four USDA beef quality grades available commercially, i.e., Prime, Choice, Select, and Standard. Correlation of all the parameters with the actual %-fat were calculated in the form of Pearson's product moment correlation coefficients (r_p) using SAS software (SAS Institute Inc., Cary, NC). The coefficients (r_p) between selected parameters and actual %-fat are presented in Table II, Table III, and Table IV. All the parameters listed in the table were significantly correlated with %-fat ($p<0.05$), assuming a normal probability distribution of the parameters. The mutual correlation coefficients among the ultrasound parameters are also shown. The correlation values are discussed in the following sections.

Correlation of Signal Parameters and %-Fat

The spectral parameter f_L (6-dB cutoff low frequency) showed good correlation with %-fat for both window sizes, 512 points (r=-0.31) and 256 points (r=-0.26) (Table II). This indirectly gives an indication of frequency dependent nature of the attenuation process. With increasing %-fat in the tissues, scattering and attenuation increase resulting in a shift of the spectrum to the lower frequencies giving a negative correlation with the f_L parameter. This is also observed in the good correlation (with %-fat) of other frequency parameters, such as f_c (center frequency) and f_p (frequency at peak power).

Table II. Correlation of actual %-fat with spectral parameters[§].

		512-point window parameters			256-point window parameters		
	%-fat	$f_{I.}$	f_C	f_P	$f_{I.}$	f_C	f_P
%-fat	1.00						
(512) $f_{I.}$	-0.31	1.00					
f_C	-0.20	0.46	1.00				
f_P	-0.33	0.75	0.62	1.00			
(256) $f_{I.}$	-0.26	0.90	0.38	0.68	1.00		
f_C	-0.18	0.48	0.78	0.65	0.48	1.00	
f_P	-0.24	0.70	0.54	0.78	0.74	0.65	1.00

[§]All the coefficient values are significant ($p<0.01$) unless otherwise specified (refer to text for the description of parameters).

The frequency-dependent attenuation parameters correlated well with the %-fat (Table III). The coefficients of correlation for the linear model parameters A_i (intercept) and A_s (slope) were 0.15 and 0.13, respectively. For the nonlinear power-law model, B_0 (coefficient) had a correlation coefficient of 0.25 and η (power of frequency dependence) did not exhibit significant levels of correlation with %-fat. This suggests that with increasing %-fat the frequency dependence of attenuation remains close to being linear. This is in contrast to some of the results for liver with fat infiltration [10]. The mutual correlation of A_i with B_0 was high (r=0.88) which can be explained by the linear frequency dependence of attenuation, where the power of frequency dependence is close to one.

Table III shows that kurtosis parameters, K_S and n_K are correlated well with the actual %-fat with correlation coefficients of –0.40 and –0.30, respectively. Also, as shown in the Figure 9, the value of K_S is high for low %-fat muscle and low for high %-fat muscle. This implies that the muscle with the low %-fat tend to have Gaussian distribution in the strengths of the scatterers while the muscle with the high %-fat tend to have uniform distribution in the strengths of the scatterers. The negative correlation of n_K with %-fat indicates that the $K_E(n)$ of tissues with low %-fat takes longer to stabilize than the $K_E(n)$ of tissues with high %-fat. It

Table III. Correlation of actual %-fat with attenuation parameters and kurtosis parameters§.

	%-fat	Attenuation Parameters				Kurtosis Parameters	
		Linear Model		Power Law Model			
		A_T	A_S	B_0	η	K_S	n_K
%-fat	1.00						
A_T	0.15	1.00					
A_S	0.13†	-0.57	1.00				
B_0	0.25	-0.88	-0.15†	1.00			
η	0.02‡	-0.64	0.55	-0.39	1.00		
K_S	-0.40	-0.08‡	-0.15	-0.17	0.00‡	1.00	
n_K	-0.30	0.00‡	-0.14†	-0.09‡	-0.04‡	0.70†	1.00

§All the coefficient values are significant ($p<0.01$) unless otherwise specified (refer to text for the description of parameters).
†$0.01<p<0.05$
‡$p>0.05$

should be noted here that in B-mode ultrasound image, the muscles with low %-fat tend to have heterogeneous texture, whereas, the muscles with high %-fat tend to have a more homogeneous texture.

Table IV shows the correlation of the parameters extracted from envelope of the signal segment. The positive correlation of the mean of the histogram of envelope (r=0.25) implies that average amplitude of the backscatter echoes from the high %-fat ribeye is higher than the average amplitude of the backscatter echoes from the low %-fat ribeye. The correlation of the rms energy is good (r=0.22) but it does not provide information that is different from H_M as seen from the observed mutual correlation value of 0.99. The peak parameters (P_1, P_2, P_3) also show good positive correlation with the actual %-fat. This could be related to the increase in scattering strength and number density with the increase in the intramuscular fat content. The peak parameters with different thresholds do not provide any additional information as their mutual correlation is very high (above 0.78).

Table IV. Correlation table of actual %-fat and envelope parameters[§].

		512-point window parameters					256-point window parameters				
	%-fat	H_M	E_G	P_1	P_2	P_3	H_M	E_G	P_1	P_2	P_3
%-fat	1.00										
(512) H_M	0.25	1.00									
E_G	0.22	0.99	1.00								
P_1	0.28	0.21	0.09[‡]	1.00							
P_2	0.29	0.18	0.08[‡]	0.91	1.00						
P_3	0.28	0.15	0.06[‡]	0.78	0.93	1.00					
(256) H_M	0.24	0.99	0.98	0.22	0.20	0.16	1.00				
E_G	0.22	0.99	0.99	0.13[†]	0.11[†]	0.09[‡]	0.99	1.00			
P_1	0.24	0.23	0.12[†]	0.89	0.79	0.65	0.22	0.12[†]	1.00		
P_2	0.31	0.26	0.16	0.85	0.86	0.74	0.25	0.16	0.91	1.00	
P_3	0.33	0.21	0.13[†]	0.76	0.80	0.73	0.21	0.14[†]	0.79	0.93	1.00

[§]All the coefficient values are significant ($p<0.01$), unless otherwise specified (refer to text for the description of parameters).
[†]$0.01<p<0.05$
[‡]$p>0.05$

Prediction Model and Validation Testing

There were a total of 14 parameters which significantly correlated ($p<0.05$) with %-fat. However, no single parameter was able to predict %-fat with acceptable accuracy. Out of 295 carcasses for which the %-fat values were available, only 8 ribeye samples had values less than 2.0 %-fat or more than 11.0 %-fat. These extreme value samples were excluded from statistical model development. Out of the remaining 287 samples, data from 200 samples were used for developing the multiple regression model for predicting %-fat and rest of the remaining 87 samples were used for validating the model.

The prediction model used six A-mode parameters: K_s, f_p (256-point window), P_a, f_p (512-point window), A_i, and A_e. The Pearson's product moment correlation and the Spearman's rank correlation between the predicted and the actual %-fat were 0.57 ($p<0.01$) and 0.55 ($p<0.01$), respectively. A regression of the predicted %-fat on the actual %-fat gave a slope of 1.37 ($p<0.01$)

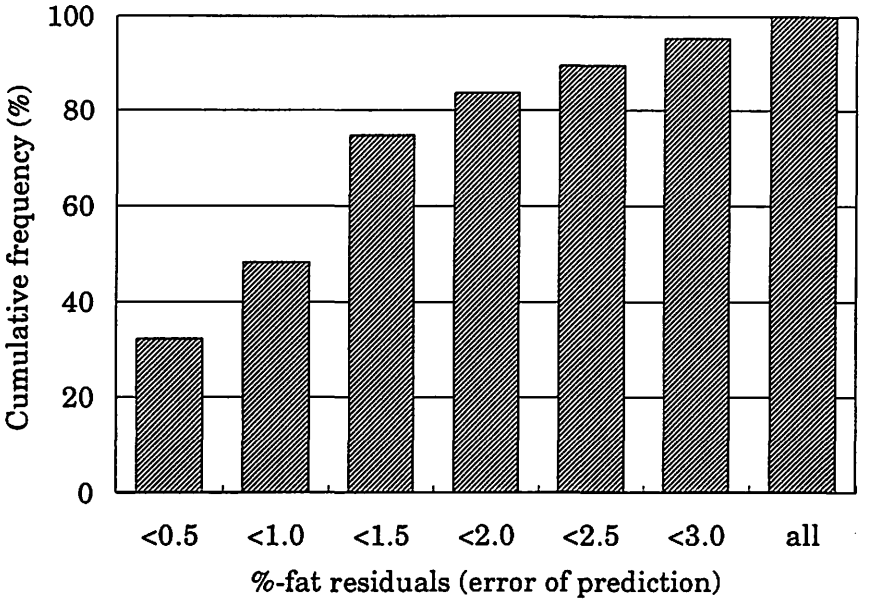

Figure 11. Cumulative frequency versus error of %-fat prediction for validation testing of the model.

and a statistically insignificant intercept. Other useful test results were a root mean square error (RMSE) of 1.33 and a coefficient of determination (R^2) of 0.33. Thus, the prediction model showed good accuracy with good correlation coefficients and low RMSE. The regression slope, however, showed some bias which could be due to the nonlinear relationship of frequency parameters at the extremes of the %-fat range. Also, for the validation the model accounted for only 33% of the variations in the actual %-fat.

Figure 11 presents the results of analysis of residuals (absolute difference between predicted and actual %-fat). Here, the residuals are grouped into different ranges and the cumulative frequencies for progressively larger residual groups are plotted for the prediction model. As seen from the figure, for 84% of the samples in the testing data set, the model predicted %-fat to within 2.0 %-fat error, and for 75% of the samples, to within 1.5 %-fat error. There were only 4 samples out of 87 for which the prediction error was more than 3.0 %-fat. However, they were predicted within 3.5 %-fat error. It was difficult to predict the extreme

cases of %-fat (particularly values close to 11.0%). This might be because there were inadequate number of samples in these groups to have sufficient representation in the model development process.

Thus, the %-fat prediction results are very encouraging and hence, scanning and application of signal processing techniques should be continued to further the process of building robust models. Ongoing research is also aimed at improving the signal-to-noise ratio of the signals acquired by using a real-time signal averager. Newer techniques of multi-parameter pattern recognition techniques such as piece-wise linear regression and artificial neural network are also being considered for improving prediction close to the extremes of the %-fat range. Also, efforts are being made to combine A-mode and B-mode ultrasound parameters for improving the prediction accuracy. We expect a significant improvement with this approach because B-mode images provide 2-dimensional tissue structure information in the form of image texture parameters while A-mode signals provide information about ultrasound tissue interaction, for example, attenuation. The ultimate goal is to incorporate a successful scheme or algorithm in a portable dedicated computerized ultrasonic system (under development at Iowa State University) for evaluation of the beef carcasses as well as live animals.

CHAPTER 7

CONCLUSION

A simple and effective A-mode signal processing techniques have been derived for characterizing intramuscular %-fat in ribeye muscle of the beef carcasses. This approach may provide an important step towards an objective grading system for beef quality. The signal parameters are empirical and physical meaning for some of the parameters is not clear. However, considering the large size of the experiment (311 carcasses), and significant correlations the approach has a great potential for non-destructively evaluating the beef quality based on intramuscular fat content.

BIBLIOGRAPHY

[1] P. N. T. Wells, Ultrasonics in clinical diagnosis, Churchill Livingsstone, Edinburgh and London, 1972.

[2] W. N. McDicken, Diagnostic ultrasonics: Principles and use of instruments, John Wiley & Sons, New York, 1976.

[3] E. J. Feleppa and M. M. Yaremko, "Ultrasonic tissue characterization for diagnosis and monitoring," *IEEE Engineering in Medicine and Biology Magazine*, pp. 18-26, 1987.

[4] J. C. Bamber and C. R. Hill, "Acoustic properties of normal and cancerous human liver-I. Dependence on pathological conditions," *Ultrasound in Med. & Biol.*, vol. 7, pp. 121-133, 1981.

[5] J. M. Thijssen, A. M. Verbeek, R. L. Romijn, D. de Wolff-Rouendaal and J. A. Oosterhuis, "Echographic differentiation of histological types of intraocular melanoma," *Ultrasound in Med. & Biol.*, vol. 17, no. 2, pp. 127-138, 1991.

[6] V. Amin, D. Wilson, R. Roberts, and G. Rouse, "Tissue characterization for beef grading using texture analysis of ultrasonic images," *Proceedings of the 1993 IEEE Ultrasonics Symposium*, pp. 969-972, 1993.

[7] V. Amin, R. Roberts, A. Patel, D. Wilson, and G. Rouse, "Ultrasound tissue characterization for quality grading of beef carcasses," *Review of Progress in Quantitative Nondestructive Evaluation*, edited by D. O. Thompson and D. E. Chimenti (Plenum, New York), to be published in vol. 14, 1994 (this issue).

[8] R. Kuc, "Ultrasonic tissue characterization using kurtosis," *IEEE Trans. on Ultrasonics, Feroelectrics, And Frequency Control*, vol. UFFC-33, no. 3, pp. 273-279, 1986.

[9] E. J. Feleppa, F. L. Lizzi, D. J. Coleman, and M. M. Yaremko, "Diagnostic spectrum analysis in ophthalmology: a physical perspective," *Ultrasound in Med. & Biol.*, vol. 12, no. 8, pp. 623-631, 1986.

[10] J. Ophir, T. H. Shawker, N. F. Maklad, J. G. Miller, S. W. Flax, P. A. Narayana, and J. P. Jones, "Attenuation estimation in reflection: progress and prospects," *Ultrasonic Imaging*, vol. 6, pp. 349-395, 1984.

[11] R. V. Haendchen, K. Ong, M. C. Fishbein, W. Zwehl, S. Meerbaum, and E. Corday, "Early differentiation of infarcted and noninfarcted reperfused myocardium in dogs by quantitative analysis of regional myocardial echo amplitudes," *Circ. Res.*, vol. 57, pp. 718-728, 1985.

[12] Oppenheim, A. V. and R. W. Schafer, Digital signal processing, Prentice Hall, Inc., Englewood Cliffs, N. J., 1975.

[13] S. M. Kay, Fundamentals of statistical signal processing, Prentice Hall, Inc., Englewood Cliffs, N. J., 1975.

[14] S. M. Kay, Modern spectral estimation, theory and application, Prentice Hall, Inc., Englewood Cliffs, N. J., 1988.

[15] C. Therrien, Discrete random signals and statistical signal processing, Prentice Hall, Inc., Englewood Cliffs, N. J., 1992.

[16] M. Insana, J. Zagzebski, and E. Modsen, "Improvements in the spectral difference method for measuring ultrasonic attenuation," *Ultrasonic imaging*, vol. 5, pp. 331-345, 1983.

[17] P. A. Narayana and J. Ophir, "On the frequency dependence of attenuation in normal and fatty liver," *IEEE Trans. On Sonics and Ultrasonics*, vol. SU-30, no. 6, pp. 379-383, 1983.

[18] D. E. Robinson, "Computer spectral analysis of ultrasonic A-mode echoes," pp. 281-286 in M. Linzer, ed. *Ultrasonic Tissue Characterization* II. National Bureau of Standards Special Publication 525. U. S. Government Printing Office, Washington, D. C., 1979.

[19] A. L. Edwards, An introduction to linear regression and correlation, second edition, W. H. Freeman and Company, New York, 1984.

[20] R. J Freund and R. C. Littell, SAS system for regression, second edition, Cary, NC: , SAS institute Inc., 1991.

[21] G. W. Snedecor and W. G. Cochran, Statistical Methods, eighth edition, Iowa State University Press, Iowa, 1989.

ACKNOWLEDGMENTS

As I have traveled along life's paths, I have been blessed with individuals who have inspired me at critical points in my life. But as I reflect on the journey thus far, I would like to recognize the following individuals:

First I would like to express my sincere gratitude to Dr. Satish Udpa and Dr. Ronald Roberts for their guidance, patience, and understanding as the major professors through out my study and research work. I would also like to thank Dr. Viren Amin for his technical advice, encouragement, and support. I would not have accomplished many of these things without his help.

Many thanks are owed to Dr. Doyle Wilson and Dr. Gene Rouse for their helpful suggestions and giving me an opportunity to work with them. I will remember the scanning trips to Windom, Minnesota and the "Tomahawk truck drivers". I would also like to acknowledge Dr. Lalita Udpa for participating on my graduate committee and for helpful comments.

My deepest gratification is expressed to my grandparents, Ambalal Patel and Jadaben Patel, who are no longer with me, for their morale support. I would like to express my love and gratitude to my grandmother, Madhuben Patel (Maji). She would have been the first person I would have wanted to see after my graduation, but unfortunately that's not possible. Mere words cannot express my admiration, love, and gratitude for my grandparents, their encouragement for higher education will always inspire me to strive for excellence and I am proud and fortunate to have all of them in my life.

This research was supported in part by research grants from USDA-CSRS, National Livestock and Meat Board, and Iowa Beef Industry Council.